Hindawi
Mathematical Problems in Engineering
Volume 2018, Article ID 2485263, 13 pages
https://doi.org/10.1155/2018/2485263

Research Article

A Dual-Observer Design for Nonlinear Suspension System Based on Feedback Linearization

Zheng Liu, Yuzhuang Zhao, and Sizhong Chen

School of Mechanical Engineering, Beijing Institute of Technology, Beijing 100081, China

Correspondence should be addressed to Yuzhuang Zhao; zyz1112@163.com

Received 25 September 2018; Revised 23 November 2018; Accepted 13 December 2018; Published 26 December 2018

Academic Editor: Nicola Caterino

A novel approach to estimate suspension state information and payload condition was developed in this article. A nonlinear quarter car model with air spring and damper was built. After verification of system observability and solvability, a certain coordinate transform was built to transform the nonlinear system into a linear one. Then a Kalman filter observer was applied. A sprung mass observer, which works cooperatively with suspension state information observer, was also designed. Designed dual-observer was verified under typical road profile and sprung mass disturbance. Compared with extended Kalman filter, the dual-observer showed better accuracy and robustness.

1. Introduction

1.1. Background. The function of the suspension system is to isolate the passenger and payload from road disturbance and maintain contact between the wheel and the road at all times, which is called "ride comfort" and "ride holding", respectively [1, 2]. Conventionally, these conflicting objectives are achieved by designing a passive suspension whose damping coefficient and stiffness curves are carefully selected for a compromised solution [3], while in recent years, there have been growing interests in the control strategy of semiactive and active suspension systems [4, 5]. Semiactive and active suspension systems can have better performance compared to conventional suspension systems due to their ability to change damping coefficient or stiffness and damping coefficient at the same time [6–8]. The performance of these control strategies strongly depends on the accuracy of vehicle parameters and state information [9], while due to system complexity, expenses, and technical limits, not all the state information can be measured directly by sensors [10] and online measurements of all the state variables of a process are rarely available. Now in industrial application, common technique to obtain state information which can not be measured directly from sensors such as vehicle body velocity is to integrate signals from accelerometers. However, such technique suffers a lot from errors caused by drift [11, 12].

1.2. Formulation of the Problem of Interest of This Investigation. In such cases, reliable information of unmeasurable variables such as vertical velocity of spring mass is obtained by applying a state observer. State observers are systems designed based on a mathematical model and are capable of reconstructing the inaccessible variables from easily available measurements [13–15]. Now most mutual observers designed for vehicle vibration state such as Kalman filter (KF) are based on linear system, while in industrial practice, most of the vehicle system has nonlinear character. Simply neglecting those nonlinear character and treating the vehicle system as a linear one can cause serious problems like the deterioration of estimation accuracy which will finally lead to poor control effect of active/semiactive suspension system.

1.3. Literature Survey. Kalman filter (KF) is an algorithm that uses a series of measurements in time domain and produces estimates of unknown variables that tend to be more precise than those based on a single measurement alone are. It is the optimal estimate for linear system models [9, 10, 16]. To apply this filtering method to nonlinear systems, many efforts are made by former researchers. Extended Kalman filter (EKF) is applied to vehicle system by Rigatos and Jurkiewicz [17, 18]. The EKF uses first order Taylor expansion to approximate the nonlinear system [19]. However, the linear

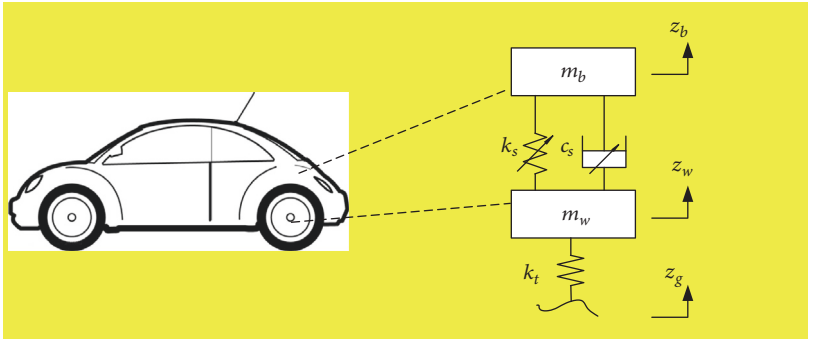

Figure 1: Nonlinear quarter car model.

system obtained through this method can only reflect the system character around the equilibrium position. When the system is severely nonlinear, it may lead to deteriorated estimation result [20]. Then Unscented Kalman filter is developed by Jeffrey Uhlmann. Researchers like Anronov and Hedrick applied UKF to vehicle system and accomplished better results compared to EKF [21, 22]. The UKF performs a stochastic linearization by performing unscented transform which uses a bunch of sigma points to approximate the mean and the variance of the system. So UKF is approved to have higher order accuracy then EKF [20]. Sliding mode theory is also used in the design of state observers [23, 24]. The sliding mode observer uses the error between the estimated state and real state to design the sliding mode surface, which can ensure that the estimated states can follow the real states [23, 25, 26]. Other newly developed observers like fuzzy observer and neural network observer do not rely on system dynamic model and their accuracy rely on large amount of training data, which sometimes is not easy to get [24, 27–30]. System identification is also considered in modern observer design. Gordon implemented online mass and stiffness identification by using recursive least-square [31]. An adaptive observer design, which was used for observer-based parameter identification in the active suspension system of an automobile, was implemented by Hedrick [32].

1.4. Scope and Contribution of This Study. The main motivation of this study is to apply a new approach of observer design to suspension system. Instead of trying to get approximation of the nonlinear system, feedback linearization transforms the nonlinear system to an observable linear one. Theoretically, the process does not affect the accuracy of the designed observer [33]. Moreover, the linearized form is easy to dealt with, which leaves much possibility for future work of implementing some mutual linear observer design technique such as Adaptive Kalman filter to nonlinear system.Then dual-observer design is introduced to the system which identify the vehicle sprung mass in real time.

1.5. Organization of the Paper. In this paper, a feedback linearization method has been implemented, which transform the original nonlinear system into an observable one by finding a specific transforming coordinate. Then the traditional linear Kalman filter algorithm can be applied in this transformed system. After each Kalman filter iteration, the linear system can be transformed back into the original system through inverse transformation, then the state information can be obtained. Payload variation is also considered in this paper. Since vehicle mass can vary significantly from one loading condition to another [34]. So we designed another Kalman filter to identify the vehicle payload by measuring the sprung mass vertical acceleration. The robustness of the system is significantly improved by exchanging the estimated results between these two observers in real time.

The paper is organized as follows: a nonlinear quarter car model is explained in Section 2; feedback linearization for above nonlinear model is introduced in the subsequent section; Kalman filter for state information observation and sprung mass identification is designed in Section 4; simulation tests are done in Section 5 and performance of above algorithm is illustrated in the same section; conclusions and future work are explained in the last section.

2. Nonlinear Quarter Car Model

Linear model can replace the nonlinear model around the operating point, out of the range, deviation cannot be ignored and the linear one is not valid. Therefore, a quarter car nonlinear model is established as shown in Figure 1.

There are two degrees of freedom of vibration in this model, vertical movement of sprung and unsprung mass. In Figure 1, m_b is sprung mass, which varies when payload changes. Sprung mass is supported by air spring whose stiffness coefficient is k_s and damping shock absorber whose damping coefficient is c_s. Unsprung mass, shown in Figure 1 as m_w, is supported by tire, which is simplified as linear model with constant stiffness coefficient k_t. z_b and z_w are displacement of sprung and unsprung mass, respectively, and road profile is denoted as z_g.

The dynamic function of this model can be described as

$$\begin{aligned} m_b\ddot{z}_b &= -F_s\left(z_b - z_w\right) - F_d\left(\dot{z}_b - \dot{z}_w\right) \\ m_w\ddot{z}_w &= F_s\left(z_b - z_w\right) + F_d\left(\dot{z}_b - \dot{z}_w\right) - k_t \cdot \left(z_w - z_g\right) \end{aligned} \tag{1}$$

where F_s is the spring force, which is the function of spring stroke, and F_d is damping force which is the function of damper stroke and stroke rate.

Table 1: Values of quarter car model parameters.

Parameters	Symbols	Values	Unit
Quarter car sprung mass	m_b	210	kg
Quarter car un-sprung mass	m_w	43	kg
Tire stiffness coefficient	k_t	2.38e5	$N.m^{-1}$
Gas polytrophic exponent	r	1.4	-
Effective section area of the piston	A_a	0.0088	m^2
Volume of the air bag	V_{sb}	0.0027	m^3
Static equilibrium pressure of the energy accumulator	P_{sb}	5.8e5	Pa
Compressing stroke damping coefficient I	c_{y1}	3430	$N{\cdot}s{\cdot}m^{-1}$
Compressing stroke damping coefficient II	c_{y2}	631	$N{\cdot}s{\cdot}m^{-1}$
Compressing stroke throttle opening rate	v_y	-0.1	$m{\cdot}s^{-1}$
Extending stroke damping coefficient I	c_{s1}	4447	$N{\cdot}s{\cdot}m^{-1}$
Extending stroke damping coefficient II	c_{s2}	1750	$N{\cdot}s{\cdot}m^{-1}$
Extending stroke throttle opening rate	v_s	0.3	$m{\cdot}s^{-1}$

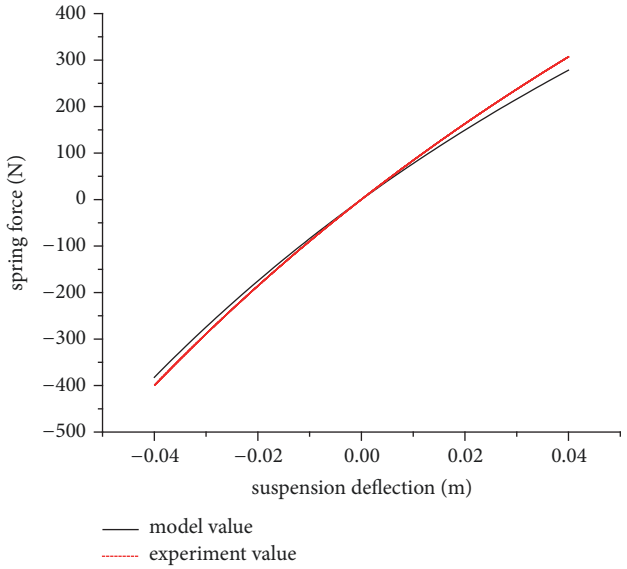

Figure 2: Characteristic of spring force.

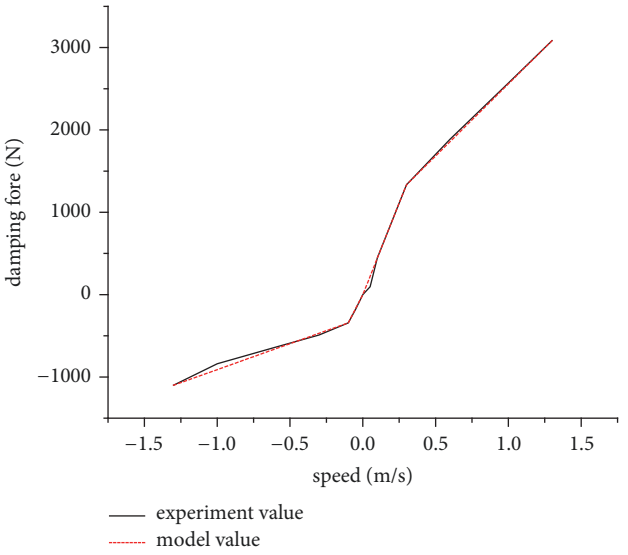

Figure 3: Characteristic of damping force.

In our system, the suspension system shows nonlinear character because of the nonlinear force generated by air spring and the damper. So models of air spring and damper are also built in this paper.

The nonlinear spring force can be described as

$$F_s = \left[1 - \frac{V_{sb}^r}{\left(V_{sb} + A_\alpha \cdot \Delta z\right)^r}\right] \cdot p_{sb} \cdot A_\alpha \tag{2}$$

where r is gas polytrophic exponent, A_a is effective section area of the piston, P_{sb} is the static equilibrium pressure of the energy accumulator, Δz is the spring stroke, and V_{sb} is volume of the air bag.

Stiffness characteristic of air suspension is shown in the Figure 2.

Piecewise function of damper property is as follows; coefficients are acquired by data fitting of experimental data,

$$F_d(v) = \begin{cases} c_{y2} \cdot \left(v - v_y\right) + c_{y1} \cdot v_y & v < v_y \\ c_{y1} \cdot v & v_y \le v < 0 \\ c_{s1} \cdot v & 0 \le v < v_s \\ c_{s2} \cdot \left(v - v_s\right) + c_{s1} \cdot v_s & v \ge v_s \end{cases} \tag{3}$$

where v_s is the throttle opening rate in extending stroke, v_y is the throttle opening rate in compressing stroke, c_{s1} and c_{s2} are damping coefficient in extending stroke, and c_{y1} and c_{y2} are damping coefficient in compressing stroke.

Characteristic of the damping force compared with experiment value is shown in Figure 3.

All the parameters used in this chapter are listed in the Table 1.

3. Feedback Linearization of Nonlinear Suspension System

The basic idea for feedback linearization is to find a proper nonlinear coordinate transformation and turn a nonlinear system into a linear system. Then traditional and well-developed linear observer algorithm can be applied to the system. Our system is a no input multioutput stochastic system and the feedback linearization method is based on differential geometry [33].

Take the following system, for example:

$$\begin{aligned} \dot{x} &= f(x) \\ y &= h(x) \end{aligned} \tag{4}$$

A linearized form can be obtained through coordinate transfer x = X(ξ).

$$\begin{aligned} \dot{\boldsymbol{\xi}} &= A\boldsymbol{\xi} + b(y) \\ y &= h(X(\boldsymbol{\xi})) = C\boldsymbol{\xi} \end{aligned} \tag{5}$$

where (A, C) is the observation matrix pair. ξ is the state vector of the transformed system.

For our certain system, considering system process noise, and measurement noise we can build the state space model for our system. Define state vector

$$x = \left[x_1, x_2, x_3, x_4\right]^T = \left[\dot{z}_b,\ \dot{z}_w,\ z_b - z_w,\ z_w - z_g\right]^T, \tag{6}$$

define measurement variable,

$$y = \left[y_1, y_2\right]^T = \left[\dot{z}_b - \dot{z}_w,\ z_b - z_w\right]^T \tag{7}$$

the reason for such measurement variable selection will be explained later in our article, and the state space model can be expressed as

$$\begin{aligned} \dot{x} &= f(x) + G \cdot w \\ y_m &= h_y(x) + v \end{aligned} \tag{8}$$

where $w = \dot{z}_g$ is the process noise and v is the measurement noise.

$$f(x) = \begin{bmatrix} -\dfrac{F_d(x_1 - x_2)}{m_b} - \dfrac{F_s(x_3)}{m_b} \\ \dfrac{F_d(x_1 - x_2)}{m_w} + \dfrac{F_s(x_3)}{m_w} - \dfrac{k_t}{m_w}x_4 \\ x_1 - x_2 \\ x_2 \end{bmatrix},$$

$$G = \begin{bmatrix} 0 \\ 0 \\ 0 \\ -1 \end{bmatrix}, \tag{9}$$

$$h_y(x) = \begin{bmatrix} h_1(x) \\ h_2(x) \end{bmatrix} = \begin{bmatrix} x_1 - x_2 \\ x_3 \end{bmatrix}$$

3.1. System Observability Verification. The system mentioned above is a 4-dimension system with a 2-dimension output. Make n=4 and m=2, where n is the dimension of the system and m is the dimension of the output function. Define observability index $L = \{l_0, \cdots, l_{k-1}\}$, where L is a K dimension real number sequence and meets

$$\begin{aligned} m = l_0 \geq \cdots \geq l_{k-1} > 0, \\ \sum_{i=0}^{k-1} l_i = n \end{aligned} \tag{10}$$

According to differential geometry theory [33], the necessary and sufficient condition for the system observability is to find a certain observability index L which can make observability matrix Q nonsingular, where

$$Q = \begin{bmatrix} dh_{(1)} \\ L_f(dh_{(2)}) \\ \vdots \\ L_f^{k-1}(dh_{(k)}) \end{bmatrix}, \tag{11}$$

$$h_{(i)} = \left[h_1,\ h_2,\ \cdots,\ h_{l_{i-1}}\right]^T$$

To find out whether rank$(Q) = n$, we need to calculate the partial derivatives and Lie derivatives of the output function.

For output function $h_1(x)$

$$dh_1 = [1,\ -1,\ 0,\ 0] \tag{12}$$

$$L_f(\mathrm{d}h_1) = \left[-\frac{\mathrm{d}F_d}{m_e},\ \frac{\mathrm{d}F_d}{m_e},\ -\frac{\mathrm{d}F_s}{m_e},\ \frac{k_t}{m_w}\right] \tag{13}$$

$$L_f^2(\mathrm{d}h_1) = \left[A_1,\ -A_1 + \frac{k_t}{m_w},\ A_2,\ -\frac{k_t}{m_w}\frac{\mathrm{d}F_d}{m_e}\right] \tag{14}$$

$$\begin{aligned} &L_f^3(\mathrm{d}h_1) \\ &= \left[A_3 + \frac{k_t}{m_w}\frac{\mathrm{d}F_d}{m_w},\ -A_3 - \frac{k_t}{m_w}\left(\frac{\mathrm{d}F_d}{m_w} + \frac{\mathrm{d}F_d}{m_e}\right),\ A_4,\ A_5\right] \end{aligned} \tag{15}$$

where detailed information about (13) to (15) can be found in Appendix, (A.1) to (A.7).

For output function $h_2(x)$

$$dh_2(x) = [0, 0, 1, 0] \tag{16}$$

$$L_f^i(dh_2) = L_f^{i+1}(dh_1), \quad i = 1, 2, 3 \tag{17}$$

With above partial derivatives and Lie derivatives, it can be easily verified that when observability index

$$L = \{l_0, l_1, l_2\} = \{2, 1, 1\} \tag{18}$$

rank$(Q) = 4$, and our nonlinear suspension system is observable.

3.2. Feedback Linearization Transfer Solving. Define,

$$
\begin{aligned}
h_{I,0} &= \begin{bmatrix} h_1 \\ h_2 \end{bmatrix}, \\
h_{II,0} &= \varnothing, \\
h_{I,1} &= h_1, \\
h_{II,1} &= h_2, \\
h_{I,2} &= h_1, \\
h_{II,2} &= h_2
\end{aligned} \tag{19}
$$

$$
\begin{aligned}
Q_{I,1} &= dh_{I,0}, \\
Q_{I,2} &= \begin{bmatrix} dh_{I,0} \\ L_f\left(dh_{I,1}\right) \end{bmatrix}, \\
Q_{I,3} &= \begin{bmatrix} dh_{I,0} \\ L_f\left(dh_{I,1}\right) \\ L_f^2\left(dh_{I,2}\right) \end{bmatrix}
\end{aligned} \tag{20}
$$

Again, according to differential geometry theory [33], the nonlinear feedback is solvable if and only if

(1)

$$
L_f^j\left(dh_{II,j}\right) \in spanQ_{I,j} + span_R\left\{L_f^j\left(dh_{I,j}\right)\right\}, \quad j = 1, \cdots, k-1 \tag{21}
$$

(2) observation matrix pair(A,C) is in condensed dual Brunovský form listed below

$$
\begin{aligned}
A &= \begin{bmatrix} 0, & E_1, & & \\ & \ddots & \ddots & \\ & & \ddots & E_{k-1} \\ & & & 0 \end{bmatrix}, \\
C &= \begin{bmatrix} C_1, & 0, & \cdots & 0 \end{bmatrix}, \\
E_i &= \begin{bmatrix} e_1, \cdots, e_{l_i} \end{bmatrix} \in R^{l_{i-1} \times l_i}
\end{aligned} \tag{22}
$$

where C_1 is a nonsingular and square matrix and e_i is the ith column of the l_{i-1}-dimensional unit matrix.

Carry output functions and Lie derivatives of output functions into above defined equations; we can easily verify that (21) is met.

And there exists a observer matrix pair (A, C) which meets (22), where

$$
A = \begin{bmatrix} 0, & 0, & 1, & 0 \\ 0, & 0, & 0, & 0 \\ 0, & 0, & 0, & 1 \\ 0, & 0, & 0, & 0 \end{bmatrix},
$$

$$
C = \begin{bmatrix} 1, & 0, & 0, & 0 \\ 0, & 1, & 0, & 0 \end{bmatrix} \tag{23}
$$

For nonlinear coordinate transfer $x = X(\xi)$, define $\partial \boldsymbol{X}/\partial \boldsymbol{\xi} = \boldsymbol{G}$ where

$$
G = \begin{bmatrix} g_1, & \cdots, & g_k \end{bmatrix} \tag{24}
$$

Then following equation must be satisfied:

$$
\begin{aligned}
Q_k g_k &= \widetilde{E}_k, \\
Q_i g_i &= \widetilde{E}_i, \\
g_i E_i &= -ad_f g_{i+1}, \\
& \qquad i = k-1, \cdots, 1
\end{aligned} \tag{25}
$$

where

$$
\begin{aligned}
\widetilde{E}_i &= \begin{bmatrix} 0, & \cdots, & \overline{E}_{i-1} \end{bmatrix}^T, \\
\overline{E}_i &= \overline{E}_{i-1} E_i, \\
\overline{E}_0 &= I
\end{aligned} \tag{26}
$$

According to the definition of generalized inverse matrix, (25) equals

$$
\begin{aligned}
g_k &= Q_k^- \widetilde{E}_k, \\
g_i &= -ad_f g_{i+1} E_i^T + Q_i^- \widetilde{E}_i \left(I - E_i E_i^T\right) \\
&\quad + \left(I - Q_i^- Q_i\right) Z_i \left(I - E_i E_i^T\right)
\end{aligned} \tag{27}
$$

where $(\cdot)^-$ is an arbitrary $\{1\}$- inverse matrix of matrix $(\cdot)$ and Z_i is an arbitrary matrix which has the same dimension as g_i.

Then we can get

$$
\frac{\partial X}{\partial \xi} = G = \begin{bmatrix} g_1, & g_2, & g_3 \end{bmatrix} = \begin{bmatrix} 0, & 0, & 0, & \dfrac{m_w}{k_t} \\ -1, & 0, & 0, & \dfrac{m_w}{k_t} \\ 0, & 1, & 0, & 0 \\ 0, & 0, & \dfrac{m_w}{k_t}, & 0 \end{bmatrix} \tag{28}
$$

Integrate above equation; we can get coordinate transfer

$$
x = X(\xi) = \begin{bmatrix} \dfrac{m_w}{k_t} \xi_4 \\ -\xi_1 + \dfrac{m_w}{k_t} \xi_4 \\ \xi_2 \\ \dfrac{m_w}{k_t} \xi_3 \end{bmatrix} \tag{29}
$$

Table 2: Sensor placement configuration for quarter vehicle nonlinear system.

measurement	Sensor placement configuration									
	①	②	③	④	⑤	⑥	⑦	⑧	⑨	⑩
$\ddot{z}_b$	●				●		●		●	
$\dot{z}_b$		●			●			●		●
$(z_b - z_w)$			●			●	●	●		
$(\dot{z}_b - \dot{z}_w)$				●		●			●	●

Table 3: Comparison of different sensor placement configurations.

Sensor configuration	System observability	Solvability under	
		Nonlinear spring force	Nonlinear damping force
①	√		
②	√		
③	√	√	
④	√		√
⑤	√		
⑥	√	√	√
⑦	√	√	
⑧	√	√	
⑨	√		
⑩	√		√

Then we can get inverse coordinate transfer

$$\xi = T(x) = \begin{bmatrix} x_1 - x_2 \\ x_3 \\ \dfrac{k_t}{m_w} x_4 \\ \dfrac{k_t}{m_w} x_1 \end{bmatrix} \tag{30}$$

3.3. Sensor Configuration Selection. Limited by technical feasibility, there are at least 10 possible sensor configurations for our system which is shown in Table 2.

In above two chapters, we choose configuration ⑥, verified its observability and solvability, and deduced the nonlinear feedback coordinate transfer.

Repeat the process of Sections 3.1 and 3.2; we can find out that though all of above sensor configurations are observable, not all of the sensor configurations are solvable. Some are not solvable at all, some are only solvable under certain limits, as shown in chart in Table 3.

As shown in Table 3, configuration ⑥ is observable and solvable when both spring force and damping force are nonlinear. That is why we choose suspension deflection and suspension deflection velocity as our measurement variable.

3.4. Kalman Filter Design. Apply the coordinate transfer to our system; we can get

$$b(y) = \dot{\xi} - A\xi = \begin{bmatrix} \dot{\xi}_1 - \xi_3 \\ \dot{\xi}_2 \\ \dot{\xi}_3 - \xi_4 \\ \dot{\xi}_4 \end{bmatrix} = \begin{bmatrix} -\dfrac{F_d(y_1)}{m_e} - \dfrac{F_s(y_2)}{m_e} \\ \dot{x}_3 \\ -\dfrac{k_t}{m_w} y_1 \\ -\dfrac{k_t}{m_w} \dfrac{F_s(y_2) + F_d(y_1)}{m_b} \end{bmatrix} \tag{31}$$

Consider process noise and measurement noise; the system state form is

$$\begin{aligned} \dot{\xi} &= A\xi + b(y) + Bw_\xi \\ y &= C\xi + v_\xi \end{aligned} \tag{32}$$

where w_ξ is process noise and v_ξ is measurement noise.

Compared with (8), the system measurement noise is determined by the measurement system, which makes

$$v_\xi = v \tag{33}$$

To find out process noise and process noise coefficient matrix B, first of all, we can assume there is no error in the measurement variables, then $b(y) = b(C\xi)$, which makes

$$\dot{\xi} = A\xi + b(Cy) + B_1 w_\xi \tag{34}$$

Compared to the coefficient of $\dot{z}_g$, we can get coefficient matrix $B_1 = [-k_t/m_w \;\; 0 \;\; 0 \;\; 0]^T$

Now considering the process noise in the system, $y = C\xi + v_\xi$.

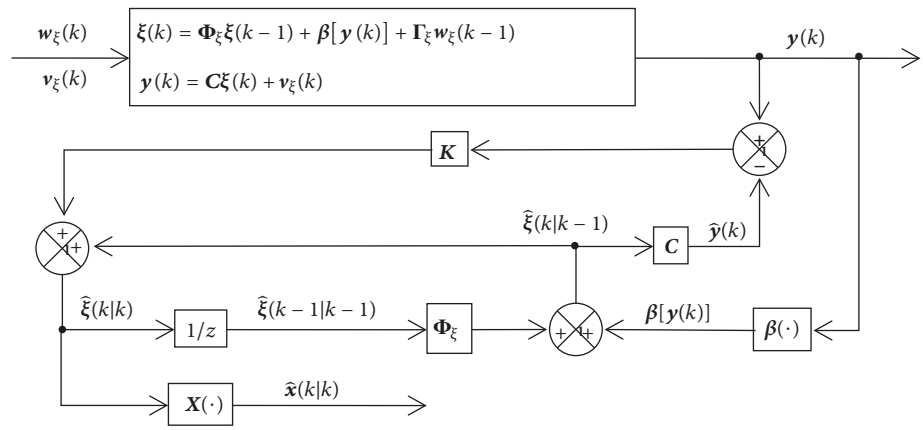

Figure 4: Flowchart of feedback linearization Kalman estimator algorithm.

According to first order Taylor expansion,

$$\dot{\xi} = A\xi + b(C\xi) + B_1 z_g \approx A\xi + b(y) + B_1 z_g - \frac{\partial b}{\partial y} v_\xi \quad (35)$$

where

$$\frac{\partial b}{\partial y} = \begin{bmatrix} -\dfrac{dF_d(y_1)}{m_e} & 1 & -\dfrac{k_t}{m_w} & -\dfrac{k_t}{m_w}\dfrac{dF_d(y_1)}{m_b} \\ -\dfrac{dF_s(y_2)}{m_e} & 0 & 0 & -\dfrac{k_t}{m_w}\dfrac{dF_s(y_2)}{m_b} \end{bmatrix}^T \quad (36)$$

Define

$$w_\xi = \begin{bmatrix} v_\xi \\ \dot{z}_g \end{bmatrix} \quad (37)$$

Then,

$$B = \begin{bmatrix} \dfrac{dF_{d0}}{m_e}, & \dfrac{dF_{s0}}{m_e}, & 0 \\ -1, & 0, & 0 \\ \dfrac{k_t}{m_w}, & 0, & -\dfrac{k_t}{m_w} \\ \dfrac{k_t}{m_w}\dfrac{dF_{d0}}{m_b}, & \dfrac{k_t}{m_w}\dfrac{dF_{s0}}{m_b}, & 0 \end{bmatrix} \quad (38)$$

where dF_{s0} is the rigid coefficient and dF_{d0} is the damping coefficient.

Then the linear Kalman filter algorithm can be applied to design the observer, which can estimate the state of ξ.

Discretize the linearized system with sample time t_s, and define $kt_s = t$, and we can get the discrete form of (32)

$$\begin{aligned} \xi(k) &= \Phi_\xi \xi(k-1) + \beta[y(k)] + \Gamma_\xi w_\xi(k-1) \\ y(k) &= C\xi(k) + v_\xi(k) \end{aligned} \quad (39)$$

where Φ_ξ, Γ_ξ, and C are matrixes with constant coefficients and $\beta(\cdot)$ is the mapping of output function.

Then the structure of feedback linearization Kalman estimator algorithm is shown in Figure 4.

4. Sprung Mass Identification

Different driving conditions cause change of sprung mass, which leads to deteriorating estimator outcome if no corresponding change is made to the estimator parameters. Therefore, we designed a sprung mass identification estimator based on linear Kalman filter, which is combined with the estimator designed in last section. Those two estimators change results in real time. Assuming the sprung mass does not change in a short time. We chose $\theta = 1/m_b$ as system state and sprung mass acceleration as measurement. The system function then is

$$\begin{aligned} \theta_{k+1} &= \theta_k + w_k \\ y_{k+1} &= H\theta_k + v_k \end{aligned} \quad (40)$$

where H is the suspension force and w_k and v_k are process noise and measurement noise, respectively.

Figure 5 is the mass estimation estimating result, and we can see that this method is working pretty well in our system.

5. Simulation and Analysis

A simulation based on MATLAB/Simulink is implemented in this section under typical road profile. To verify the accuracy and efficiency of our designed feedback linearize Kalman filter estimator (FL-KF), a comparison is made between FL-KF and extended Kalman filter (EKF).

The road profile is grade-B random road excitation determined in ISO; vehicle speed is kept at 10m/s.

Figures 6–10 show the comparison of estimation result of FL-KF and EKF. To better evaluate the accuracy of the designed estimator, an accuracy index is introduced,

$$accuracy = \left[1 - \frac{\sqrt{\sum_{k=1}^{N} (x(k) - \hat{x}(k))^2}}{\sqrt{\sum_{k=1}^{N} (x(k))^2}}\right] \times 100\% \quad (41)$$

where x is the system state, $\hat{x}$ is the estimated system state, and N is the quantity of the number of the sample. The closer the index gets to the value of 1, the more precise the estimation result is.

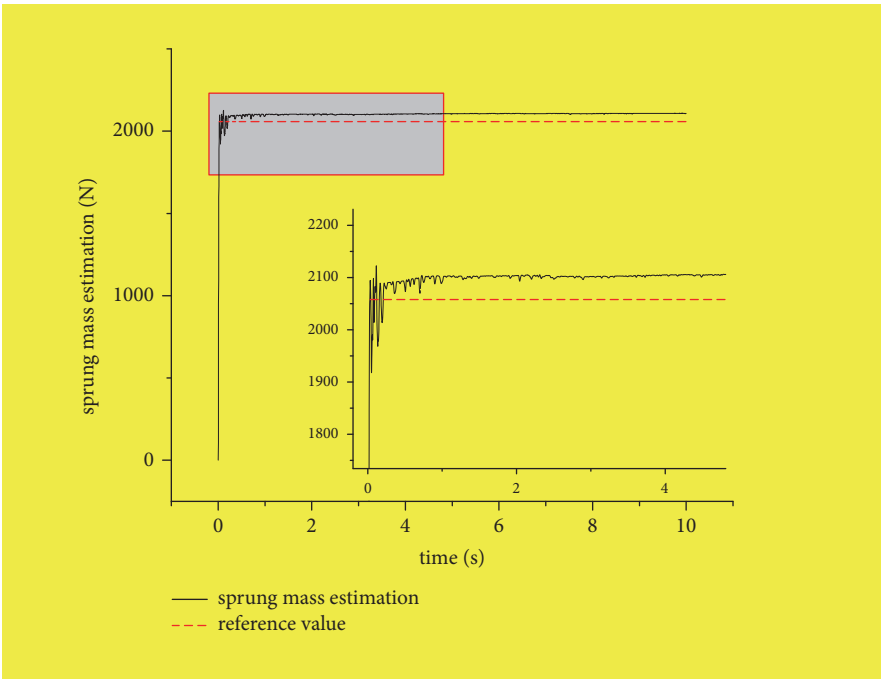

Figure 5: Result of sprung mass estimation with zoomed window.

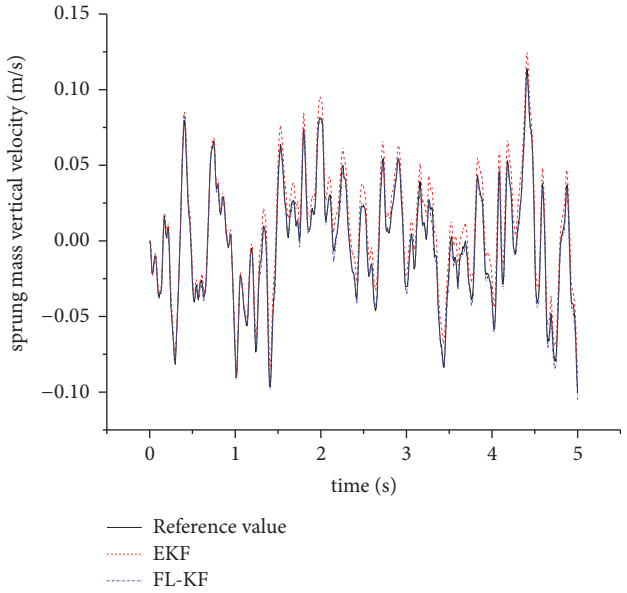

Figure 6: Sprung mass velocity estimation comparison.

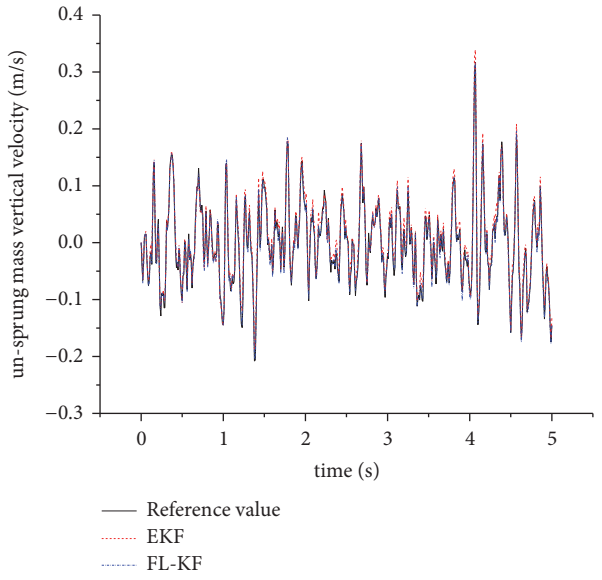

Figure 7: Unsprung mass velocity estimation comparison.

Error analysis is plotted in Figure 11, where V_ms is the sprung mass vertical velocity and V_mu is the unsprung mass vertical velocity. It can be seen that the results of FL-KF show better accuracy compared with the results of EKF.

From Figures – and Table 4 we can find out that FL-KF has better accuracy than EKF in the estimation of all five parameters listed in the table. Differences are more obvious in the estimation results of vertical velocity of sprung/unsprung mass. That is because other three parameters are either part of the measurement vector or derivative of the measurement vector.

To better verify the success of the observer, simulation under ISO grad A and grade C road is also implemented, accuracy index of which compared with the result of grad B road is listed in the Table 5. The vehicle speed is kept at 10m/s in all sets of simulations.

From data in Table 5. We can find out that the designed observer is valid under different road level excitations ranging from grade-A level to grade C level. The difference between

Table 4: Symbol meanings and accuracy index of EKF and FL-KF observer.

parameters	symbols	Accuracy index under EKF	Accuracy index under FL-KF
Vertical velocity of sprung mass	V_ms	70.8	92.0
Vertical velocity of un-sprung mass	V_mu	79.8	90.0
Suspension deflection velocity	V_sus	85.9	90.0
Vertical acceleration of sprung mass	A_ms	85.2	89.4
Suspension deflection	D_sus	96.6	96.9

Table 5: Accuracy index of EKF and FL-KF observer under different road level excitation.

	ISO grade-A road		ISO grade-B road		ISO grade-C road	
	Accuracy index of state estimation /%					
symbols	EKF	FL-KF	EKF	FL-KF	EKF	FL-KF
V_ms	77.5	94.3	70.8	92.0	62.5	90.1
V_mu	84.2	92.4	79.8	90.0	73.1	88.6
V_sus	91.3	93.0	85.9	90.0	84.7	88.3
A_ms	88.7	91.6	85.2	89.4	83.2	88.9
D_sus	96.9	97.2	96.6	96.9	92.7	93.1

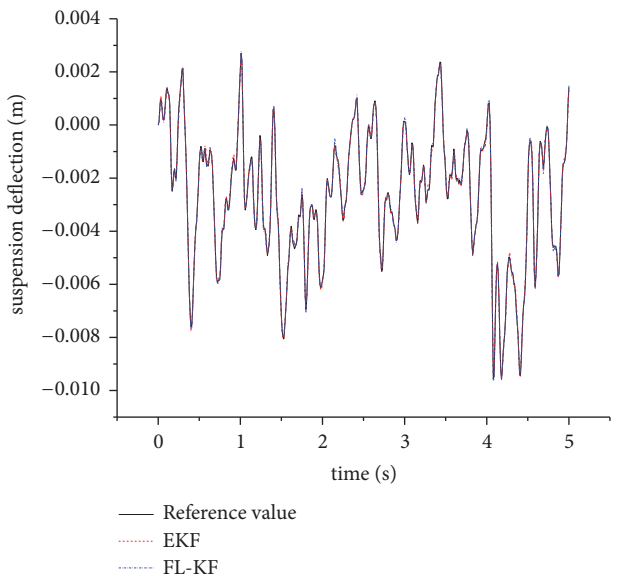

Figure 8: Suspension deflection estimation comparison.

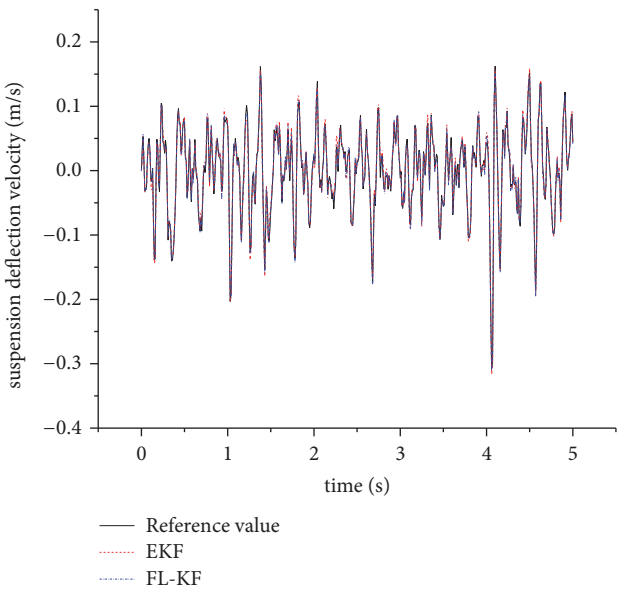

Figure 9: Suspension deflection velocity estimation comparison.

EKF and FL-KF observers gets larger when random road excitation gets severer, that is because the nonlinear character of the suspension system is more obvious when the system is far from the equilibrium position.

To verify the efficiency of our designed estimator under different vehicle load conditions, a sprung mass disturbance (plus 20%, which is 42kg) is given to the initial sprung mass value of the estimator. Road level of the simulation is ISO grade-B level and speed of the vehicle is kept at 10m/s. The outcome of our designed estimator is compared with the outcome of a feedback linearize Kalman filter without sprung mass estimator.

Figures 12–17 and Table 6 show the result of estimators with and without sprung mass identification filter. FL-KL is the result of our designed feedback linearization dual Kalman filter and FL-KF-NoME is the result of a feedback linearization single Kalman filter without sprung mass identification estimator. Results show that our designed estimator

Table 6: Accuracy index of FL-KF-NoME and FL-KF observer.

parameters	symbols	Accuracy index of FL-KF-NoME	Accuracy index of FL-KF
Vertical velocity of sprung mass	V_ms	16.9	92.0
Vertical velocity of un-sprung mass	V_mu	50.1	90.0
Suspension deflection velocity	V_sus	90.0	90.0
Vertical acceleration of sprung mass	A_ms	80.1	89.4
Suspension deflection	D_sus	96.9	96.9

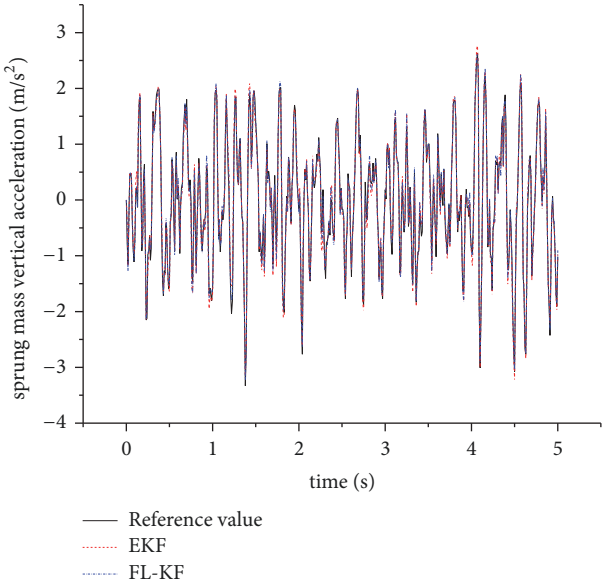

Figure 10: Sprung mass acceleration estimation comparison.

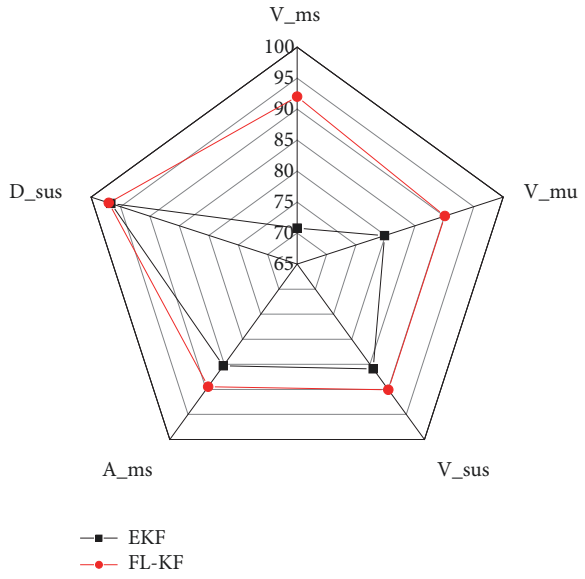

Figure 11: Error analysis for random road condition.

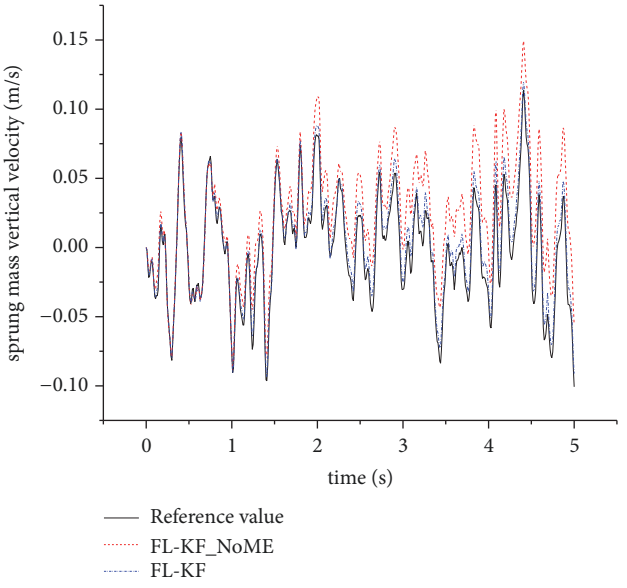

Figure 12: Sprung mass velocity estimation comparison.

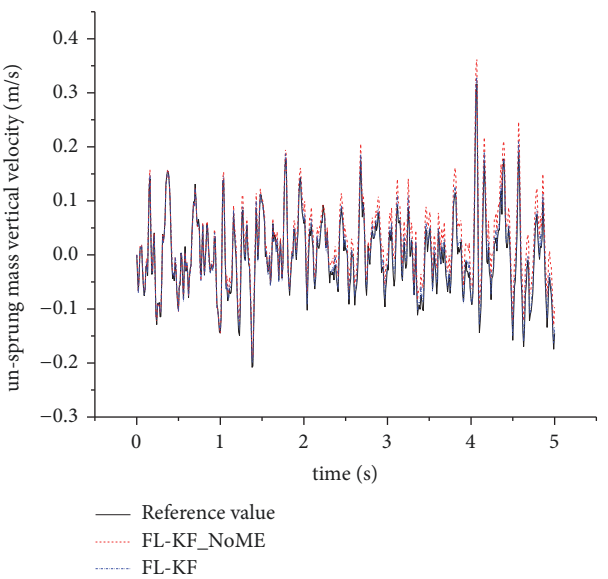

Figure 13: Unsprung mass velocity estimation comparison.

is much more accurate for sprung mass and unsprung mass velocity estimating when the payload changes, while feedback linearization Kalman filter with and without sprung mass identification estimator does not show much accuracy dif-

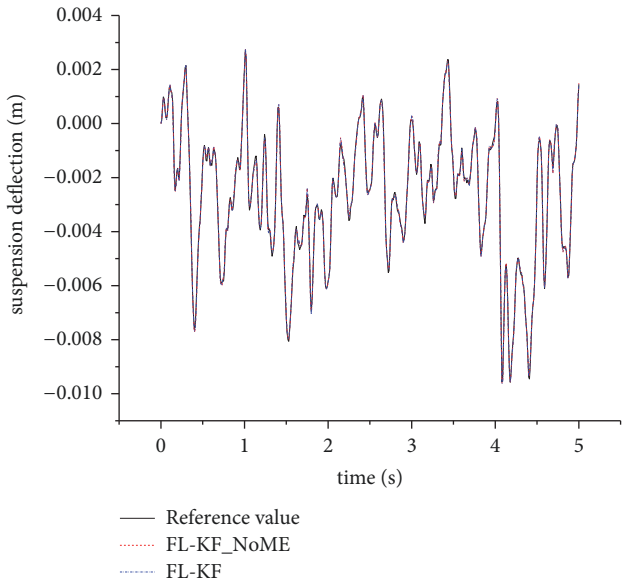

Figure 14: Suspension deflection estimation comparison.

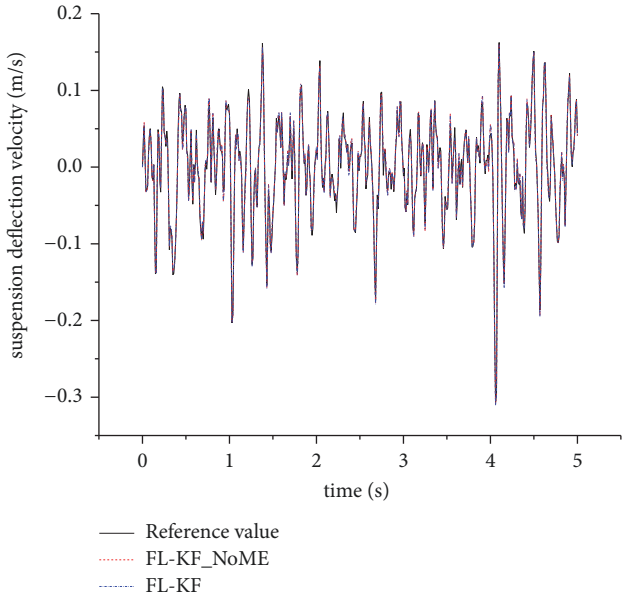

Figure 15: Suspension deflection velocity estimation comparison.

ference when estimating suspension deflection, suspension deflection velocity, and sprung mass acceleration. That is because suspension deflection and suspension deflection velocity are part of the measurement vector; sprung mass acceleration is the derivative of sprung mass velocity; sprung mass velocity of two estimators shares almost the same trend.

6. Conclusion

In this paper, a feedback linearization observer with sprung mass estimator is designed based on differential geometry.

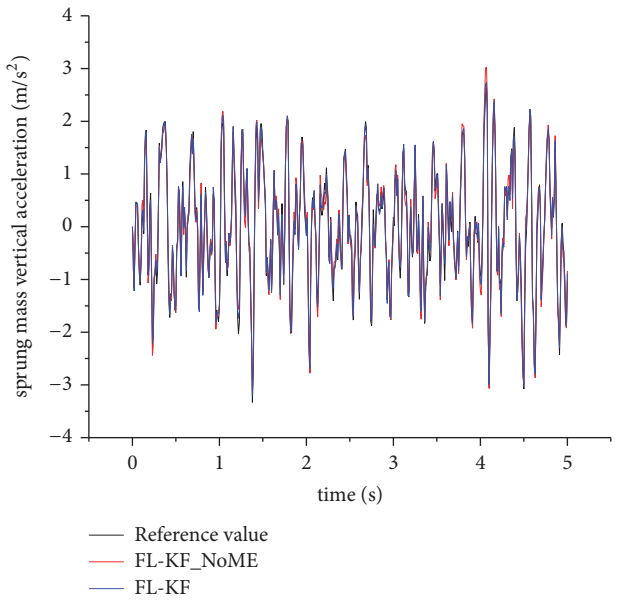

Figure 16: Sprung mass acceleration estimation comparison.

A nonlinear suspension system model is built and transformed into linear observable form, and then linear Kalman filter algorithm is applied to this transformed linear model. Efficiency and accuracy of feedback linearization observer are verified under typical road profile. Compared with EKF observer, feedback linearization observer has better performance. Sprung mass estimator is designed and its performance is verified; its necessity is verified by comparing estimation result of feedback linearization observer with and without sprung mass estimator under typical road profile. Results show that the sprung mass estimator can improve the accuracy of the observer significantly.

There are still some important issues that deserve future research; state observer should be designed for full vehicle suspension system; control algorithm for semiactive suspension system combined with state observer should be developed.

Appendix

$$m_e = \frac{m_b \times m_w}{m_b + m_w},$$

$$\mathrm{d}F_d = \frac{\mathrm{d}}{\mathrm{d}\left(x_1 - x_2\right)} F_d, \tag{A.1}$$

$$\mathrm{d}F_s = \frac{\mathrm{d}}{\mathrm{d}x_3} F_s,$$

$$d^{i+1}F_d = \frac{d}{d\left(x_1 - x_2\right)} d^i F_d,$$

$$d^{i+1}F_s = \frac{d}{dx_3} d^i F_s, \tag{A.2}$$

$$i = 1, 2, 3,$$

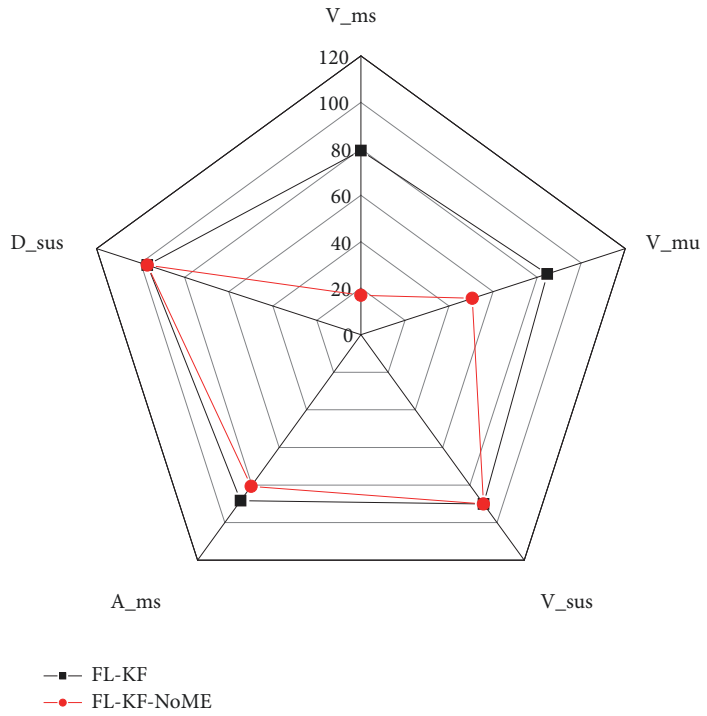

Figure 17: Error analysis for random road condition.

$$A_1 = \frac{d^2F_d}{m_e}\left(\frac{F_d}{m_e} + \frac{F_s}{m_e} - \frac{k_t}{m_w}x_4\right) + \left(\frac{dF_d}{m_e}\right)^2 - \frac{dF_s}{m_e}, \quad (A.3)$$

$$A_2 = \frac{dF_d}{m_e}\frac{dF_s}{m_e} - \frac{d^2F_s}{m_e}(x_1 - x_2), \quad (A.4)$$

$$A_3 = -\frac{dF_d}{m_e}A_1 + A_2 - \frac{d^3F_d}{m_e}\left(\frac{F_d}{m_e} + \frac{F_s}{m_e} - \frac{k_t}{m_w}x_4\right)^2 - 3\frac{d^2F_d}{m_e}\frac{dF_d}{m_e}\left(\frac{F_d}{m_e} + \frac{F_s}{m_e} - \frac{k_t}{m_w}x_4\right) + \left(\frac{d^2F_d}{m_e}\frac{dF_s}{m_e} - \frac{d^2F_s}{m_e}\right)\cdot(x_1 - x_2) - \frac{k_t}{m_w}\frac{d^2F_d}{m_e}x_2 \quad (A.5)$$

$$A_4 = -\frac{dF_s}{m_e}A_1 - \left(\frac{F_d}{m_e} + \frac{F_s}{m_e} - \frac{k_t}{m_w}x_4\right)\left(\frac{d^2F_d}{m_e}\frac{dF_s}{m_e} - \frac{d^2F_s}{m_e}\right) + \left[\frac{dF_d}{m_e}\frac{d^2F_s}{m_e} - \frac{d^3F_s}{m_e}(x_1 - x_2)\right]\cdot(x_1 - x_2) + \frac{k_t}{m_w}\frac{dF_s}{m_w}, \quad (A.6)$$

$$A_5 = \frac{k_t}{m_w}\left[A_1 + \frac{d^2F_d}{m_e}\left(\frac{F_d}{m_e} + \frac{F_s}{m_e} - \frac{k_t}{m_w}x_4\right) - \left(\frac{k_t}{m_w}\right)\right], \quad (A.7)$$

Data Availability

The data used to support the findings of this study are included within the article.

Conflicts of Interest

The authors declare that there are no conflicts of interest regarding the publication of this paper.

Acknowledgments

This work is supported by the National Nature Science Foundation of China (Grants nos. 51375046 and 51205021).

References

[1] M. Ahmadian, *Editors' Perspectives: Road Vehicle Suspension Design, Dynamics, And Control. Vehicle System Dynamics*, vol. 49, no. (1-2): pp. 3-28, 2011.

[2] H. E. Tseng and D. Hrovat, "State of the art survey: active and semi-active suspension control," *Vehicle System Dynamics*, vol. 53, no. 7, pp. 1034–1062, 2015.

[3] V. Sankaranarayanan, E. M. Emekli, L. Güvenç et al., "Semi-active suspension control of a light commercial vehicle," *IEEE/ASME Transactions on Mechatronics*, vol. 13, no. 5, pp. 598–604, 2008.

[4] X.-L. Zhang, T. Zhang, J. Nie, and L. Chen, "A Semiactive Skyhook-Inertance Control Strategy Based on Continuously Adjustable Inerter," *Shock and Vibration*, vol. 2018, 2018.

[5] S. Han, Z. Chao, and X. Liu, "A Semiactive and Adaptive Hybrid Control System for a Tracked Vehicle Hydropneumatic

Suspension Based on Disturbance Identification," *Shock and Vibration*, vol. 2017, no. 2, pp. 1–12, 2017.

[6] M. C. Smith and G. W. Walker, "Performance limitations and constraints for active and passive suspensions: A mechanical multi-port approach," *Vehicle System Dynamics*, vol. 33, no. 3, pp. 137–168, 2000.

[7] M. Demic and D. Diligenski, "Numerical simulation of shock absorbers heat load for semi-active vehicle suspension system," *THERMAL SCIENCE*, vol. 20, no. 5, pp. 1725–1739, 2016.

[8] A. Concilio, M. C. De Simone, Z. B. Rivera, and D. Guida, "A new semi-active suspension system for racing vehicles," *FME Transactions*, vol. 45, no. 4, pp. 578–584, 2017.

[9] J. Cuadrado, D. Dopico, J. A. Perez, and R. Pastorino, "Automotive observers based on multibody models and the extended Kalman filter," *Multibody System Dynamics*, vol. 27, no. 1, pp. 3–19, 2012.

[10] M. Doumiati, A. Victorino, D. Lechner, G. Baffet, and A. Charara, "Observers for vehicle tyre/road forces estimation: Experimental validation," *Vehicle System Dynamics*, vol. 48, no. 11, pp. 1345–1378, 2010.

[11] U.-X. Tan, K. C. Veluvolu, W. T. Latt, C. Y. Shee, C. N. Riviere, and W. T. Ang, "Estimating displacement of periodic motion with inertial sensors," *IEEE Sensors Journal*, vol. 8, no. 8, pp. 1385–1388, 2008.

[12] R. L. Boroschek and D. Legrand, "Tilt motion effects on the double-time integration of linear accelerometers: An experimental approach," *Bulletin of the Seismological Society of America*, vol. 96, no. 6, pp. 2072–2089, 2006.

[13] V. S. Deshpande, B. Mohan, P. D. Shendge, and S. B. Phadke, "Disturbance observer based sliding mode control of active suspension systems," *Journal of Sound and Vibration*, vol. 333, no. 11, pp. 2281–2296, 2014.

[14] G. Tang, J. Li, C. Ding, and Y. Zhang, "Sprung mass identification of suspension in a simplified model," *SAE Technical Papers*, vol. 1, 2014.

[15] D. Ning, S. Sun, F. Zhang, H. Du, W. Li, and B. Zhang, "Disturbance observer based Takagi-Sugeno fuzzy control for an active seat suspension," *Mechanical Systems and Signal Processing*, vol. 93, pp. 515–530, 2017.

[16] Y. Fan, H. Ren, S. Chen, and Y. Zhao, "Observer design based on nonlinear suspension model with unscented kalman filter," *Journal of Vibroengineering*, vol. 17, no. 7, pp. 3844–3855, 2015.

[17] G. Rigatos, P. Siano, and S. Pessolano, "Design of active suspension control system with the use of Kalman filter-based disturbances estimator," *Cybernetics and Physics*, vol. 1, no. 4, pp. 279–294, 2012.

[18] A. Jurkiewicz, J. Kowal, and K. Zając, "Extended Kalman filter in 2S1 tracked vehicle system with hybrid control," *Solid State Phenomena*, vol. 248, pp. 69–76, 2016.

[19] J. C. Alvarez, "Estimation of the longitudinal and lateral velocities of a vehicle using extended Kalman filters," 2006.

[20] S.-S. Yim, J.-H. Seok, and J.-J. Lee, "State estimation of the nonlinear suspension system based on nonlinear Kalman filter," in *Proceedings of the 2012 12th International Conference on Control, Automation and Systems, ICCAS 2012*, pp. 720–725, Republic of Korea, October 2012.

[21] H. Hamann, J. K. Hedrick, S. Rhode, and F. Gauterin, "Tire force estimation for a passenger vehicle with the Unscented Kalman Filter," in *Proceedings of the 25th IEEE Intelligent Vehicles Symposium, IV 2014*, pp. 814–819, USA, June 2014.

[22] S. Antonov, A. Fehn, and A. Kugi, "Unscented Kalman filter for vehicle state estimation," *Vehicle System Dynamics*, vol. 49, no. 9, pp. 1497–1520, 2011.

[23] J. He and C. Zhang, "Fault Reconstruction Based on Sliding Mode Observer for Nonlinear Systems," *Mathematical Problems in Engineering*, vol. 2012, Article ID 451843, 22 pages, 2012.

[24] D. Xu, B. Jiang, M. Qian, and J. Zhao, "Terminal Sliding Mode Control Using Adaptive Fuzzy-Neural Observer," *Mathematical Problems in Engineering*, vol. 2013, Article ID 958958, 8 pages, 2013.

[25] J. Stéphant, A. Charara, and D. Meizel, "Evaluation of a sliding mode observer for vehicle sideslip angle," *Control Engineering Practice*, vol. 15, no. 7, pp. 803–812, 2007.

[26] R. K. Dixit and G. D. Buckner, "Sliding mode observation and control for semiactive vehicle suspensions," *Vehicle System Dynamics*, vol. 43, no. 2, pp. 83–105, 2005.

[27] E. Kim, "A fuzzy disturbance observer and its application to control," *IEEE Transactions on Fuzzy Systems*, vol. 10, no. 1, pp. 77–84, 2002.

[28] F. Abdollahi, H. Talebi, and R. Patel, "A stable neural network observer with application to flexible-joint manipulators," in *Proceedings of the 9th International Conference on Neural Information Processing*, pp. 1910–1914, Singapore, 2009.

[29] S. N. Huang, K. K. Tan, and T. H. Lee, "Further result on a dynamic recurrent neural-network-based adaptive observer for a class of nonlinear systems," *Automatica*, vol. 41, no. 12, pp. 2161-2162, 2005.

[30] C.-S. Tseng and C.-K. Hwang, "Fuzzy observer-based fuzzy control design for nonlinear systems with persistent bounded disturbances," *Fuzzy Sets and Systems*, vol. 158, no. 2, pp. 164–179, 2007.

[31] T. J. Gordon, "Suspension System Identification Based on Impulse-Momentum Equations," *Vehicle System Dynamics*, vol. 29, supp 1, pp. 598–618, 1998.

[32] R. Rajamani and J. K. Hedrick, "Adaptive observer for active automotive suspensions," in *Proceedings of the 1993 American Control Conference Part 3 (of 3)*, pp. 706–710, June 1993.

[33] M. Hou and A. C. Pugh, "Observer with linear error dynamics for nonlinear multi-output systems," *Systems Control Letters*, vol. 37, no. 1, pp. 1–9, 1999.

[34] B. Pence, J. Hays, H. K. Fathy, C. Sandu, and J. Stein, "Vehicle sprung mass estimation for rough terrain," *International Journal of Vehicle Design*, vol. 61, no. 1-4, pp. 3–26, 2013.